Measurement of radon and xenon binding to a cryptophane molecular host

David R. Jacobson[a,1], Najat S. Khan[a,1], Ronald Collé[b], Ryan Fitzgerald[b], Lizbeth Laureano-Pérez[b], Yubin Bai[a], and Ivan J. Dmochowski[a,2]

[a]Department of Chemistry, University of Pennsylvania, 231 South 34th Street, Philadelphia, PA 19104; and [b]Ionizing Radiation Division, Physical Measurements Laboratory, National Institute of Standards and Technology, Gaithersburg, MD 20899

Xenon and radon have many similar properties, a difference being that all 35 isotopes of radon ([195]Rn–[229]Rn) are radioactive. Radon is a pervasive indoor air pollutant believed to cause significant incidence of lung cancer in many geographic regions, yet radon affinity for a discrete molecular species has never been determined. By comparison, the chemistry of xenon has been widely studied and applied in science and technology. Here, both noble gases were found to bind with exceptional affinity to tris-(triazole ethylamine) cryptophane, a previously unsynthesized water-soluble organic host molecule. The cryptophane–xenon association constant, $K_a = 42,000 \pm 2,000$ M^{-1} at 293 K, was determined by isothermal titration calorimetry. This value represents the highest measured xenon affinity for a host molecule. The partitioning of radon between air and aqueous cryptophane solutions of varying concentration was determined radiometrically to give the cryptophane–radon association constant $K_a = 49,000 \pm 12,000$ M^{-1} at 293 K.

host–guest chemistry | supramolecular chemistry | xenon biosensing

Radon and xenon were isolated by Ramsay and coworkers more than one century ago, but since that time only the chemistry of xenon has received much attention. Xenon can be harvested from the atmosphere and has wide-ranging applications, from plasma televisions to ion propulsion systems for spacecraft. Radioactive ^{133}Xe is used as a tracer for measuring physiological blood flow (1) and also in detecting long-range fallout from nuclear weapons testing (2). Stable isotope [129]Xe has a spin-half nucleus that can be hyperpolarized to generate very large signals for MRI (3). Host molecules have been identified that bind xenon with high affinity (4), motivating further technological applications. Much less studied is radon, a radioactive noble gas that occurs as an intermediate species in the decay chain of uranium-238, an element ubiquitous in Earth's crust. Epidemiological studies indicate that indoor accumulation of radon may cause a 5–31% increase in lung cancer risk per 100 Bq m^{-3} exposure (5). In Europe, such a level corresponds to 2% of all cancer deaths (5). The imperative to detect and remediate indoor radon motivates the study of radon chemistry, as do other scientific applications such as radon emission related to seismic activity (6). Prior radon-chemical studies have focused on adsorption of the gas to bulk substrates (7) such as charcoal, silica gel, and ice, and on the formation of radon halides (8). Radon hydrates have also been found to incorporate into the crystal lattices of SO_2 and H_2S hydrates (8). Until now, no discrete molecular species has been shown to bind radon, presenting an exciting frontier in noble gas research and host–guest chemistry.

Radon is 10–15% larger by van der Waals volume than xenon ($V_{Xe} \approx 42$ Å^3, $V_{Rn} \approx 47$ Å^3) (9) and exhibits higher polarizability ($\alpha_{Xe} = 4.044$ Å^3, $\alpha_{Rn} = 5.3$ Å^3) (10), which should promote binding to void spaces. These observations led us to examine binding of radon to a cryptophane organic host molecule that has well-established xenon affinity (4). Cryptophane-A, consisting of two cyclotriguaiacylene caps joined by three ethylene linkers, has been shown to encapsulate xenon reversibly as a host–guest complex (11). Recent X-ray crystallographic studies have shown

that the internal volume of trisubstituted cryptophane-A derivatives can vary by more than 20%, depending on the size of the encapsulated guest (12). Several cryptophane-A derivatives have been synthesized and shown by isothermal titration calorimetry (ITC), fluorescence quenching, and NMR studies to exhibit xenon association constants as high as $33,000 \pm 3,000$ M^{-1} at 293 K in phosphate-buffered water (13–16). Herein, we report a previously unsynthesized cryptophane-A derivative, tris-(triazole ethylamine) cryptophane (TTEC), with superior xenon-binding characteristics. A sensitive radiometric assay was developed for measuring radon binding to the same cryptophane.

Results

Synthesis. The synthetic route leading to TTEC (compound **6**) is outlined in Fig. 1 and here briefly described. A list of reagents, general methods, and synthetic procedures are provided in *SI Text*. Tripropargyl cryptophane **4** was synthesized in 10 steps in 4% overall yield according to literature procedure and matched the reported physical constants and NMR spectrum (14). We synthesized 2-azidoethylamine in 93% yield, also following literature precedent (17). Reaction of **4** with three equivalents of 2-azidoethylamine was achieved via copper(I)-mediated $[3 + 2]$ Huisgen cycloadditions (18–21) to give the water-soluble TTEC (**6**). TTEC was purified by HPLC (Fig. S1 provides representative trace) and isolated in 75% yield. TTEC identity was confirmed by ^{1}H, ^{13}C, and hyperpolarized ^{129}Xe NMR spectroscopy (Fig. S2), in addition to matrix-assisted laser desorption/ionization mass spectrometry.

Xenon Binding. To study the binding of xenon to TTEC, we utilized an ITC protocol previously developed in our laboratory (14). The experiments were performed by titrating TTEC in phosphate buffer (20 mM, pH 7.5) at 293 K with saturated xenon-in-water solution (5.05 mM at 1 atm, determined from the literature, ref. 22). The association constant was measured to be $K_a = 42,000 \pm 2,000$ M^{-1} at 293 K, which is the highest xenon affinity measured for any synthetic or naturally occurring host molecule. The cited uncertainty interval for K_a is a standard uncertainty, assumed to correspond to a standard deviation, whose principal component was the uncertainty of the enthalpogram fit. Specifically, fitting of the enthalpogram (molar heat evolved vs. molar ratio, Fig. 2) yielded thermodynamic parameters for the encapsulation: $\Delta H = -14.96 \pm 0.30$ kJ mol^{-1}; $-T\Delta S = -10.97$ kJ mol^{-1} at 293 K. Note that enthalpic and entropic components contributed similarly to the Gibbs free energy of xenon binding at 293 K ($\Delta G =$
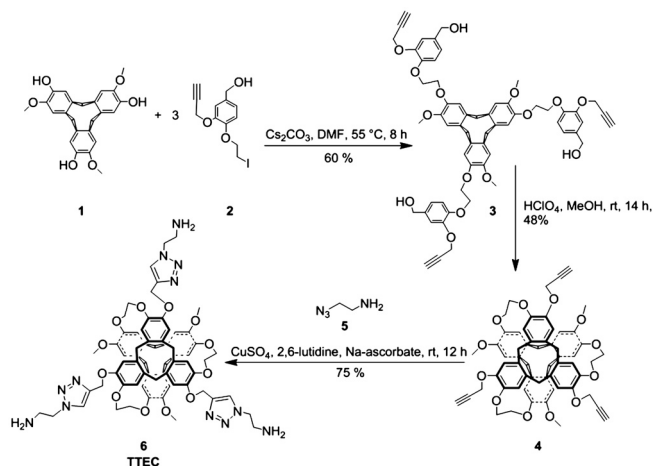
Fig. 1. Synthesis of TTEC; top view shown.

-25.93 kJ mol^{-1}), which is believed to incorporate contributions from the dissolution of the clathrate water structure that surrounds xenon in solution, the release of one or more water molecules from the cryptophane cavity, and the noncovalent dispersion interactions between bound xenon and TTEC.

Radon Binding. Studies of radon binding used ^{222}Rn evolved from the decay of ^{226}Ra in four capsules, akin to National Institute of Standards and Technology standards disseminated as SRM 4973 (23) and consisting of polyethylene-encapsulated ^{226}Ra solution. These capsules generate a radium-free radon solution from decay of the radium and diffusion of the gaseous radon out of the capsules (24), and have been used to produce very small quantities of radon for use in calibrating environmental standards—e.g., those of drinking water. In particular, only about two femtomoles of
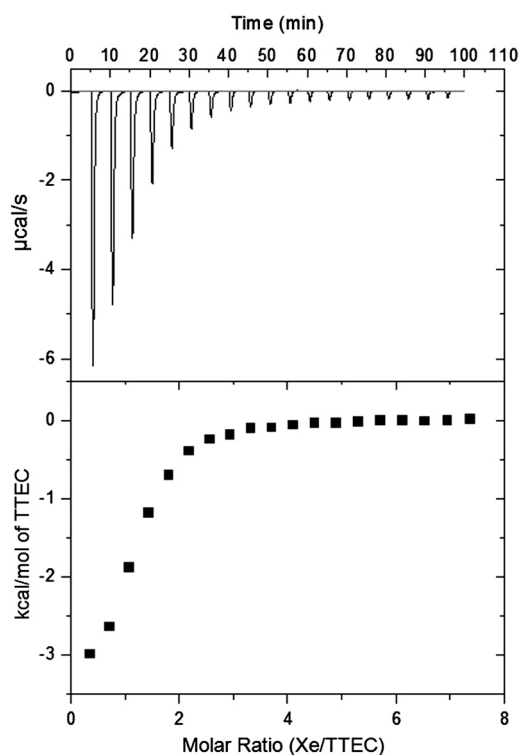

Fig. 2. Enthalpogram of xenon binding to TTEC. Saturated aqueous xenon solution (5.05 mM) was titrated into 140 μM TTEC in phosphate buffer (20 mM, pH 7.5) at 293 K.

radon were available for use in our studies, rendering impractical the fluorescence quenching and ITC methods we previously used to measure xenon binding to cryptophane in water (14). Instead, we devised a method (Fig. 3) wherein the binding of radon to TTEC could be measured radiometrically by liquid scintillation, a technique with detection efficiency approaching five due to equilibrated radon progeny (25). A related technique, involving gas-phase activity measurement, has been used to determine the partition of radon between water and various organic liquids (26). Radon partitions between gas and liquid phases according to a known ratio: the Ostwald solubility coefficient, L (27), for that liquid and temperature. Cryptophane dissolved into the liquid phase of such a system acts as a radon sink and perturbs the system away from the Ostwald value in proportion to the binding affinity. Radon was allowed to partition between the gas and liquid phases for 30–40 min, with intermittent mixing. Subsequent sampling of the liquid phase allowed determination of the "apparent partition coefficient," and from that K_a. We begin with the standard expression of K_a:

$$K_a = \frac{[\text{Bound}]}{[\text{TTEC}]_{\text{free}}[\text{Rn}]_{\text{free}}}.$$

Because $[\text{Rn}] \ll [\text{TTEC}]$ (femtomole vs. micromole quantities), the simplification was made that $[\text{TTEC}]_{\text{free}} \approx [\text{TTEC}]$. Therefore,

$$K_a = \frac{A_B}{A_{\text{free}}} \frac{1}{[\text{TTEC}]}$$

where A_B and A_{free} are the bound and free radon activities in solution, which were not independently measured. We have the definition of the Ostwald solubility coefficient,

$$L = \frac{[\text{Rn}]_{\text{free}}}{[\text{Rn}]_g} = \frac{A_{\text{free}} V_g}{A_g V_l},$$

where V_g and V_l are the gas and liquid phase volumes and A_g the gas-phase radon activity. Defining the *apparent* partition coefficient, L',

$$L' = \frac{(A_{\text{free}} + A_B) V_g}{A_g V_l},$$

we arrive at the relationship

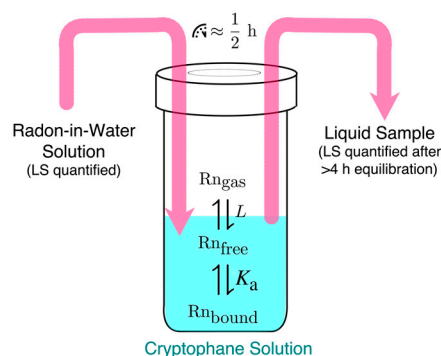$$L' = L K_a [\text{TTEC}] + L. \quad \text{[1]}$$

Fig. 3. Diagrammatic representation of the radon binding affinity measurement, which exploits the partition of radon between aqueous and gaseous phases. L is the Ostwald coefficient of gas partition and K_a is the radon association constant to be determined.

Jacobson et al.

From liquid scintillation (LS) counting before and after exposure to cryptophane, we determined A_g and $(A_{\text{free}} + A_B)$, which in turn yielded L'. Our L' vs. [TTEC] data were fit by linear regression to Eq. **1** (Fig. 4). By this method, the affinity of TTEC for radon was found to be $K_a = 49{,}000 \pm 12{,}000$ M^{-1} at 293 K. The standard uncertainty given here for K_a derived from the 95% confidence intervals on the parameters of fit to the apparent partition coefficient vs. TTEC concentration series (Eq. **1** and Fig. 4). The uncertainties in the liquid scintillation measurements used to determine the radon concentrations were negligible. These data were well fit by a linear model, with $R^2 = 0.87$. Radon activity measured for reaction vessels containing no cryptophane deviated from this line, as expected when the [Rn] ≪ [TTEC] condition no longer holds.

Discussion

From these experiments, radon was found to bind TTEC with a free energy of binding 0.4 kJ/mol more negative than in the case of xenon (−26.3 vs. −25.9 kJ/mol). However, radon is also more soluble in water solution than xenon and therefore liberates less free energy upon desolvation (−20.71 kJ/mol, Rn vs. −23.18 kJ/mol, Xe; estimate from ref. 28). Accounting for this difference in desolvation energy, we estimate that supramolecular interactions of the TTEC–Rn complex (e.g., balance of improved dispersion interactions and entropic cost of confinement) produce a free energy of binding 2.9 kJ/mol stronger than in the TTEC–Xe complex. Our previous crystallographic study showed that the internal volume of trisubstituted cryptophane-A derivatives bound to Xe is roughly 87 Å^3 and can expand to approximately 100 Å^3 to accommodate a much larger (71 Å^3) CDCl$_3$ guest (12). We can assume that TTEC bound to either Xe or Rn adopts a very similar geometry to the previous **4**-Xe crystal structure (12) (Fig. 5). As evidenced by this structure, Xe underfills the cryptophane cavity, interacting over tenths of angstroms with the phenyl carbon atoms in both cyclotriguaiacylene caps. The somewhat larger, more polarizable Rn atom is expected to exhibit stronger van der Waals interactions with TTEC than Xe, as supported by the measured enhancement in free energy of binding.

Despite the institution of government-sponsored detection and remediation programs in many countries (29), contemporary assessments show that radon exposure remains the second leading cause of lung cancer, after smoking, in the United States (30, 31). Although the environmental health risks posed by radon are well recognized, studies of radon binding to well-defined synthetic or biological targets have not been performed; studies have

Fig. 5. Structure of **4**–Xe complex determined from X-ray crystallography (12). Van der Waals radii are shown for Xe (blue sphere) and carbon atoms of one pair of opposing phenyl groups. Hydrogen atoms have been removed for clarity. Rn is expected to bind to the same site in TTEC, while occupying 10–15% more of the interior cavity volume.

tended to focus on the association of radon progeny, not radon itself (32). Challenges in this work have been to obtain pure ^{222}Rn and make binding measurements on very small quantities of material. In the current study, pure radon was obtained by sealing ^{226}RaCl$_2$ solution inside of polyethylene capsules permeable only to the gaseous emanation. These capsules, placed in a sealed 10.6-mL water-filled vessel, generated a useful concentration of ^{222}Rn within roughly 1 wk as a steady state was approached. This solution provided sufficient ^{222}Rn for tens of binding measurements. This method requires the radium-filled capsules to be properly sealed, and all ^{222}Rn manipulations must be performed using gas-tight syringes inside of a laboratory fume hood. With these precautions, this method has broad utility for the study of radon binding to many different biological samples, biomolecules, or other small-molecule hosts.

The concepts of supramolecular chemistry (33, 34) can be usefully applied to the study of radon binding. For example, many organic cavitands should bind radon with appreciable affinity, based on radon's considerable polarizability and molecular volume, which is similar to that of dichloromethane. This study showed that a water-soluble cryptophane-A derivative binds radon with considerable affinity. Indeed, TTEC may provide a nearly optimal cavity for radon as its internal volume (*ca.* 90 Å^3, assuming modest expansion from the average **4**-Xe structure) (12) is approximately twice the radon atomic volume (35). Furthermore, in lieu of three ethylamine groups, tripropargylated **4** can be reacted with a wide variety of water-solubilizing azido linkers that may fine tune the host-noble gas interaction (12–14).

Considering our previous study of the analogous tris-(triazole propionic acid) cryptophane (14), it is striking that a tris-carboxylate to tris-amine substitution at the cryptophane periphery increased the Xe association constant from 17,000 to 42,000 M^{-1} at 293 K. In order to explore the role of electrostatic interactions, we investigated xenon binding to TTEC at pH 2.5 and pH 7.5. In a previous study with a hexa-acetate cryptophane (its six acid moieties positioned at the cryptophane periphery), the ^{129}Xe NMR chemical shift decreased by approximately 3.5 ppm in aqueous solution as the pH was increased from 4 to 5 (36). In contrast, hyperpolarized ^{129}Xe NMR spectroscopy with TTEC at 298 K (Figs. S2 and S3) gave comparable cryptophane-bound chemical shifts at pH 2.5 (63.3 ppm) and pH 7.5 (63.6 ppm), which is indicative of very similar Xe-binding environments within the cryptophane. Over this pH range, the compound went from a state of predominantly triple protonation at pH 2.5 to mostly single protonation at pH 7.5 while remaining in solution (Fig. S4). Slightly higher Xe-binding affinity was observed by ITC at pH 7.5 than pH 2.5 ($K_a = 42{,}000 \pm 2{,}000$ M^{-1} vs. $K_a = 34{,}000 \pm 1{,}000$ M^{-1} at 293 K, Fig. S5). Thus, it appears that electrostatic interactions,

Fig. 4. Apparent partition coefficient, L', as a function of cryptophane concentration; ○ represent reaction vessels that contained no cryptophane; ■ represent a series of increasing cryptophane concentrations in the nonsaturated regime, fitted to Eq. **1**.

as well as other effects such as cryptophane solvation and water occupancy, are responsible for the enhanced Xe binding observed in TTEC.

Conclusion

The development of high-affinity Xe-binding cages is an area of active investigation and is critical to the burgeoning field of xenon biosensing (16, 37, 38). Synthetic host molecules designed to bind xenon in cells or in vivo must compete against a wide variety of biological substrates. Xenon is lipophilic and exhibits affinity for cavities in macromolecular interiors. Xenon's lipophilic behavior has been shown from its partition with long-chain hydrocarbons (39, 40) and from its in vitro (41) and in vivo (42) partition with fatty tissue. Xenon binding to myoglobin has been well characterized by NMR spectroscopy (43, 44) and X-ray crystallography (45), and metmyoglobin-Xe association constants have been measured to be approximately 200 and 10 M^{-1} (45, 46). Comparable affinities have been determined for other naturally occurring sites in hemoglobin (44), lipoxygenase (47), and lipid transfer protein (48), as well as specially designed hydrophobic cavities in T4 lysozyme (49), ribose-binding protein (50), and other examples (51, 52). We showed previously that xenon binds water-soluble cryptophanes approximately 1.5-fold less avidly in human plasma than in aqueous buffer solution (14). Thus, the design of higher affinity xenon-binding molecules such as TTEC extends the range of possible biological applications. Biologically targeted cryptophanes are under development as potential ^{129}Xe MRI contrast agents, as demonstrated by xenon biosensors for the prototypical biotin-avidin interaction (53, 54) and other proteins (55–57), as well as preliminary cell studies (58–60). This demonstration of radon binding to cryptophane raises similar possibilities of molecularly functionalized radon binders for biological, environmental, and materials applications involving radon delivery, sequestration, or detection.

Finally, it is significant that xenon and radon showed similarly tight binding for a well-defined molecular cavity (TTEC). This similarity suggests that radon, which like xenon is known to be lipophilic (26, 61), also binds with appreciable affinity to many proteins, surfactants, and small air spaces in the lung and other regions of the body. Radiometric binding methods developed in the course of this work will enable quantitative comparisons of radon binding to various biomolecular targets, as a means of assessing environmental health risk. Such information may ultimately be useful in developing more effective mitigation strategies for this indoor pollutant.

Methods

Xenon-Binding Study. ITC was performed using a MicroCal VP-ITC titration microcalorimeter. TTEC was dissolved in phosphate buffer (20 mM, pH 7.5) and the concentration (140 μM) was determined by UV-visible spectroscopy according to the extinction coefficient of TTEC at 280 nm ($\varepsilon_{280} = 12{,}400$ M^{-1} cm^{-1}). The preparation of saturated aqueous xenon solution and the determination of xenon concentration at 293 K were performed following the same methodology reported previously (14, 22). The titrations were carried out at 293 K; 1.8 mL of the TTEC in 20 mM phosphate buffer was placed in the calorimeter cell, and the saturated xenon-water solution was loaded into the microsyringe.

The titration was performed by the sequential addition of 15 μL aliquots of xenon solution (for a total of 19 injections) at 5-min intervals. The heat of reaction per injection (microcalories per second) was determined by integration of the peak areas (ORIGIN 7.0, MicroCal software). The values of the binding enthalpy (ΔH°), the stoichiometry of binding (n), and the association constant (K_a) were obtained from fitting the heat evolved per mole of xenon injected versus the xenon/TTEC molar ratio using the same software. Three control experiments (Figs. S6 and S7) were performed with each phosphate buffer (20 mM) at pH 7.5 or pH 2.5: (i) saturated xenon solution titrated into buffer; (ii) water titrated into TTEC-buffer solution; and (iii) water titrated into buffer to determine the heats of dilution. Processes i and ii were subtracted from, and iii was added back to, the corresponding TTEC-xenon-binding enthalpogram before curve fitting.

Radon-Binding Study. Radon was generated from 63 kBq ^{226}Ra in four polyethylene capsules submersed in a water-filled 10.6-mL vessel sealed with an aluminum-lined septum. Radon was allowed to accumulate in the water for 8 d prior to the experiment. The emanation fraction (i.e., the ratio of accumulated ^{222}Rn to the total generated from ^{226}Ra decay) for the capsules was about 30%. Stock TTEC solution concentration (48.3 μM) was determined by UV-visible spectroscopy and radon-in-water solution concentration (1.002 pM) by LS counting. Glass vials (1.1-mL Chromacol screw top, Supelco) sealed with polytetrafluoroethylene septa were filled by micropipette with varying concentrations of cryptophane solution (0.49–5.29 nmol in 120 μL; six concentrations, each in duplicate, and three null trials) with radon-in-water solution (400 μL) from the generator, by 10-mL glass, gas-tight Hamilton syringe. The rest of the vial was left as airspace. The samples were incubated for 30–40 min at 293 K; each vial was subjected to two 5-s vortex mixings, one each at the beginning and end of the incubation. A 400-μL sample was withdrawn from each vial and injected beneath the surface of approximately 19-mL LS cocktail that consisted of a commercial scintillation fluid (Ultima GAB, PerkinElmer) having a 5% water fraction in a 22-mL Al-foil-lined glass LS vial. LS counting was done using automated equipment after allowing time for radon to equilibrate with its daughter nuclides. Each sample was counted for 1 h in two apparatuses with different operational parameters (Beckman Coulter; Wallac, PerkinElmer). All liquid transfers by micropipette and syringe, as well as the precise volumes of the vials, were quantified gravimetrically.

The radon determinations were based on well-established LS procedures for the assay of gravimetrically determined aliquots of aqueous solutions containing radon in radioactive equilibrium with its short-lived daughter products (23). Raw LS data were corrected for background (<0.3% correction), for the radon content in the airspace above the cocktail in the LS vials (approximately 0.7% correction), and for radioactive decay to a common reference time. Counting was initiated after a minimum of 4 h to ensure that the radon daughters were in radioactive equilibrium. Each source was measured for 20 min over a period of 0.2–4.9 d on 6–10 occasions. The corrected net counting rates were observed to decay with the radon half-life, indicating that there was no radium leakage from the capsules. Corrected data were fitted to Eq. **1** by least-squares linear regression using MATLAB (Mathworks) to obtain K_a and L.

1. Obrist WD, Thompson HK, Wang HS, Wilkinson WE (1975) Regional cerebral blood flow estimated by 133-xenon inhalation. *Stroke* 6:245–256.
2. Perkins R, Casey L (1996) *Radioxenons: Their Role in Monitoring a Comprehensive Test-Ban Treaty* (US Department of Energy, Richland, VA), DOE/RL-96–51.
3. Oros A, Shah NJ (2004) Hyperpolarized xenon in NMR and MRI. *Phys Med Biol* 49:R105–R153.
4. Brotin T, Dutasta J (2009) Cryptophanes and their complexes: Present and future. *J Chem Rev* 109:88–130.
5. Darby S, et al. (2005) Radon in homes and risk of lung cancer: Collaborative analysis of individual data from 13 European case-control studies. *BMJ* 330:223–227.
6. Ghosh D, Deb A, Sengupta R (2009) Anomalous radon emission as precursor of earthquake. *J Appl Geophys* 69:67–81.
7. Eichler B, Zimmermann HP, Gäggeler HW (2000) Adsorption of radon on ice surfaces. *J Phys Chem A* 104:3126–3131.
8. Avrorin VV, Krasikova RN, Nefedov VD, Toropova MA (1982) The chemistry of radon. *Russ Chem Rev* 51:12–20.
9. Runeberg N, Pyykkö PI (1998) Relativisitc pseudopotential calculations on Xe$_2$, RnXe and Rn$_2$: The van der Waals properties of radon. *Int J Quantum Chem* 66:131–140.
10. Lide DR (2002) *CRC Handbook of Chemistry and Physics* (CRC, New York), pp 10–165.
11. Bartik K, Luhmer M, Dutasta J, Collet A, Reisse J (1998) ^{129}Xe and ^{1}H NMR study of the reversible trapping of xenon by cryptophane-A in organic solution. *J Am Chem Soc* 120:784–791.
12. Taratula O, Hill PA, Khan NS, Carroll PJ, Dmochowski IJ (2010) Crystallographic observation of "induced fit" in a cryptophane host–guest model system. *Nat Commun* 1:148.
13. Fogarty HA, et al. (2007) A cryptophane core optimized for xenon encapsulation. *J Am Chem Soc* 129:10332–10333.
14. Hill PA, Wei Q, Eckenhoff RG, Dmochowski IJ (2007) Thermodynamics of xenon binding to cryptophane in water and human plasma. *J Am Chem Soc* 129:9262–9263.
15. Hill PA, Wei Q, Troxler T, Dmochowski IJ (2009) Substituent effects on xenon binding affinity and solution behavior of water-soluble cryptophanes. *J Am Chem Soc* 131:3069–3077.

16. Fairchild RM, et al. (2010) A water-soluble Xe@cryptophane-111 complex exhibits very high thermodynamic stability and a peculiar (129)Xe NMR chemical shift. *J Am Chem Soc* 132:15505–15507.

17. Angelos S, Yang Y-W, Patel K, Stoddart JF, Zink JI (2008) pH-Responsive supra-molecular nanovalves based on cucurbit[6]uril pseudorotaxanes. *Angew Chem Int Ed* 47:2222–2226.

18. Tornoe CW, Christensen C, Meldal M (2002) Peptidotriazoles on solid phase: [1,2,3]-Triazoles by regiospecific copper(I)-catalyzed 1,3-dipolar cycloadditions of terminal alkynes to azides. *J Org Chem* 67:3057–3064.

19. Kolb HC, Finn MG, Sharpless KB (2001) Click chemistry: Diverse chemical function from a few good reactions. *Angew Chem Int Ed* 40:2004–2021.

20. Rostovtsev VV, Green LG, Fokin VV, Sharpless KB (2002) A stepwise Huisgen cycloaddi-tion process: Copper(I)-catalyzed regioselective "ligation" of azides and terminal alkynes. *Angew Chem Int Ed* 41:2596–2599.

21. Punna S, Kuzelka J, Wang Q, Finn MG (2005) Head-to-tail peptide cyclodimerization by copper-catalyzed azide-alkyne cycloaddition. *Angew Chem Int Ed* 44:2215–2220.

22. Clever HL (1979) *Krypton, Xenon and Radon, Solubility Data Series*, (Pergamon, Ox-ford), 2.

23. National Institute of Standards and Technology (2005) Certificate, Standard Reference Material 4973. *Radon-222 Emanation Standard* (National Institute of Standards and Technology, Gaithersburg, MD).

24. Collé R (1995) A precise determination of the ^{222}Rn half-life by 4πα-β liquid scintillation measurements. *Radioact Radiochem* 6:16–29.

25. Collé R, Kishore R (1997) Update on the NIST radon-in-water standard generator: Its performance efficacy and long-term stability. *Nucl Instrum Methods Phys Res A* 391:511–528.

26. Schubert M, Lehmann K, Paschke A (2007) Determination of radon partition coeffi-cients between water and organic liquids and their utilization for the assessment of subsurface NAPL contamination. *Sci Total Environ* 376:306–316.

27. Battino R (1984) The Ostwald coefficient of gas solubility. *Fluid Phase Equilib* 15:231–240.

28. Scharlin P, Battino R, Silla E, Tuñón I, Pascual-Ahuir JL (1998) Solubility of gases in water: Correlation between solubility and the number of water molecules in the first solvation shell. *Pure Appl Chem* 70:1895–1904.

29. Cole LA (1993) *Element of Risk: The Politics of Radon* (Am Assoc for the Advancement of Science, Washington, DC).

30. Pawel DJ, Puskin JS (2004) The U.S. Environmental Protection Agency's assessment of risks from indoor radon. *Health Phys* 87:68–74.

31. Lugg A, Probert D (1997) Indoor radon gas: A potential health hazard resulting from implementing energy-efficiency measures. *Appl Energy* 56:93–196.

32. Evans HH, et al. (1993) Interlaboratory comparison of the effects of radon on L5178Y cells: Dose contribution of radon daughter association with cells. *Radiat Res* 136:48–56.

33. Lehn J-M (1995) *Supramolecular Chemistry* (Wiley, New York), pp 1–271.

34. Davis AV, Yeh RM, Raymond KN (2002) Supramolecular assembly dynamics. *Proc Natl Acad Sci USA* 99:4793–4796.

35. Mecozzi S, Rebek J (1998) The 55% solution: A formula for molecular recognition in the liquid state. *Chem Eur J* 4:1016–1022.

36. Berthault P, et al. (2010) Effect of pH and counterions on the encapsulation proper-ties of xenon in water-soluble cryptophanes. *Chem Eur J* 16:12941–12946.

37. Kim BS, et al. (2008) Water soluble cucurbit[6]uril derivative as a potential Xe carrier for Xe-129 NMR-based biosensors. *Chem Commun* 24:2756–2758.

38. Taratula O, Dmochowski IJ (2010) Functionalized ^{129}Xe contrast agents for magnetic resonance imaging. *Curr Opin Chem Biol* 14:97–104.

39. Clever HL (1958) The solubility of xenon in some hydrocarbons. *J Phys Chem* 62:375–376.

40. Graziano G (2003) Solvation thermodynamics of xenon in n-alkanes, n-alcohols and water. *Biophys Chem* 105:371–382.

41. Yeh SY, Peterson RE (1963) Solubility of carbon dioxide, krypton, and xenon in lipids. *J Pharm Sci* 52:453–458.

42. Andersen AM, Ladefoged J (1967) Partition coefficient of 133-xenon between various tissues and blood in vivo. *Scand J Clin Lab Invest* 19:72–78.

43. Rubin SM, Spence MM, Goodson BM, Wemmer DE, Pines A (2000) Evidence of nonspecific surface interactions between laser-polarized xenon and myoglobin in solution. *Proc Natl Acad Sci USA* 97:9472–9475.

44. Tilton RF, Kuntz ID (1982) Nuclear magnetic-resonance studies of Xe-129 with myoglo-bin and hemoglobin. *Biochemistry* 21:6850–6857.

45. Tilton RF, Kuntz ID, Petsko GA (1984) Cavities in proteins—structure of a metmyoglo-bin-xenon complex solved to 1.9-Å. *Biochemistry* 23:2849–2857.

46. Ewing GJ, Maestas S (1970) Thermodynamics of absorption of xenon by myoglobin. *J Phys Chem* 74:2341–2344.

47. Bowers CR, et al. (1999) Exploring surfaces and cavities in lipoxygenase and other proteins by hyperpolarized xenon-129 NMR. *J Am Chem Soc* 121:9370–9377.

48. Dubois L, et al. (2004) Probing the hydrophobic cavity of lipid transfer protein from *Nicotiana tabacum* through xenon-based NMR spectroscopy. *J Am Chem Soc* 126:15738–15746.

49. Quillin ML, Breyer WA, Griswold IJ, Matthews BW (2000) Size versus polarizability in protein-ligand interactions: Binding of noble gases within engineered cavities in phage T4 lysozyme. *J Mol Biol* 302:955–977.

50. Lowery TJ, Rubin SM, Ruiz EJ, Pines A, Wemmer DE (2004) Design of a conformation-sensitive xenon-binding cavity in the ribose-binding protein. *Angew Chem Int Ed* 43:6320–6322.

51. Groger C, et al. (2003) NMR-spectroscopic mapping of an engineered cavity in the I14A mutant of HPr from *Staphylococcus carnosus* using xenon. *J Am Chem Soc* 125:8726–8727.

52. Rubin SM, Lee SY, Ruiz EJ, Pines A, Wemmer DE (2002) Detection and characterization of xenon-binding sites in proteins by Xe-129 NMR spectroscopy. *J Mol Biol* 322:425–440.

53. Spence MM, Rubin SM, Dimitrov IE (2001) Functionalized xenon as a biosensor. *Proc Natl Acad Sci USA* 98:10654–10657.

54. Spence MM, et al. (2004) Development of a functionalized xenon biosensor. *J Am Chem Soc* 126:15287–15294.

55. Chambers JM, et al. (2009) Cryptophane xenon-129 nuclear magnetic resonance biosensors targeting human carbonic anhydrase. *J Am Chem Soc* 131:563–569.

56. Schlundt A, et al. (2009) A xenon-129 biosensor for monitoring MHC-peptide interac-tions. *Angew Chem Int Ed Engl* 48:4142–4145.

57. Wei Q, et al. (2006) Designing ^{129}Xe NMR biosensors for matrix metalloproteinase detection. *J Am Chem Soc* 128:13274–13283.

58. Seward G, Bai Y, Khan NS, Dmochowski IJ (2011) Cell-compatible, integrin-targeted cryptophane-^{129}Xe NMR biosensors. *Chem Sci* 2:1103–1110.

59. Seward GK, Wei Q, Dmochowski IJ (2008) Peptide-mediated cellular uptake of cryptophane. *Bioconjug Chem* 19:2129–2135.

60. Boutin C, et al. (2011) Hyperpolarized ^{129}Xe NMR signature of living biological cells. *NMR Biomed*, 10.1002/nbm.1686.

61. Nussbaum E, Hursh JB (1958) Radon solubility in fatty acids and triglycerides. *J Phys Chem* 62:81–84.

CHEMISTRY

ENVIRONMENTAL SCIENCES